Floquet scattering approach to electron transport for a quantum wire under longitudinally polarized electromagnetic field irradiation

2005 J. Phys.: Condens. Matter 17 6663

(http://iopscience.iop.org/0953-8984/17/42/007)

INSTITUTE OF PHYSICS PUBLISHING JOURNAL OF PHYSICS: CONDENSED MATTER

J. Phys.: Condens. Matter **17** (2005) 6663–6673 doi:10.1088/0953-8984/17/42/007

Floquet scattering approach to electron transport for a quantum wire under longitudinally polarized electromagnetic field irradiation

Guanghui Zhou[1,2,3,4] **and Yuan Li**[2]

[1] CCAST (World Laboratory), PO Box 8730, Beijing 100080, People's Republic of China
[2] Department of Physics, Hunan Normal University, Changsha 410081, People's Republic of China
[3] International Center for Materials Physics, Chinese Academy of Sciences, Shenyang 110015, People's Republic of China

E-mail: ghzhou@hunnu.edu.cn

Received 18 June 2005, in final form 25 August 2005
Published 7 October 2005
Online at stacks.iop.org/JPhysCM/17/6663

Abstract

We theoretically study the electron transport property for a semiconductor quantum wire irradiated under a longitudinally polarized electromagnetic field within a finite range. We obtain the non-perturbative solutions of the single-electron time-dependent Schrödinger equation both inside and outside the field-irradiated region of the wire according to the Floquet theorem. A general infinite matrix equation which determines the Floquet scattering coefficients is derived straightforwardly through the wavefunction matching scheme at the two interfaces between regions with and without field irradiation. The examples of numerically calculated transmission dependence on the electron incident energy for different field parameters exhibit both Fano and Rabi resonances, and the structure of the transmission is sensitive to the field parameters of amplitude and frequency as well as the irradiation length.

1. Introduction

Since the increasingly progressive arts and crafts of nano-technologies allow researchers to realize some real mesoscopic systems in the laboratory, mesoscopic physics has been extensively studied in recent years. In the fabrication process one can confine a two-dimensional electron gas (2DEG) in an ultra-narrow channel on a GaAs/$Al_xGa_{1-x}As$ heterojunction by applying gate-controlled confinement potential and obtain a two-dimensional quantum point contact (quantum wire) [1] or even an ideal one-dimensional interacting electron system [2]. Depending on the nature of the materials, quantum wires with a length up to a few

[4] Address for correspondence: Department of Physics, Hunan Normal University, Changsha 410081, People's Republic of China.

microns may still be comparable to the Fermi wavelength of electrons. In the ballistic regime and at low temperatures the quantum coherent effect will dominate the electron transport properties of these mesoscopic systems. One of the most important features is that, as the width of a quantum wire varies, the conductance shows a histogram structure and each step has a height of $2e^2/h$ or integer multiples of it [3].

The electron transport properties of a quantum wire formed on a 2DEG can be affected by many factors. The presence of disorder in a quantum wire generally leads to a suppression of the conductance plateaus below integer values [4], and the interaction of electrons induces transport anomalies [5]. However, there has been growing interest in the time-dependent transport for mesoscopic systems in recent years (see, for example, the recent review article [6] and references therein), such as those in the presence of a time-dependent potential modulation [7] for quantum wires and quantum pumping [8] for quantum dots. Furthermore, many features have been observed [9] experimentally and predicted theoretically for both quantum wires [10–14] and quantum wells [15, 16] when the system is irradiated under an external electromagnetic (EM) field. The technique of applying an external field is of particular interest, since no additional current and voltage probes have to be attached to the sample that may disturb the system's properties.

In this paper, we theoretically study the multi-photon processes of a quantum wire irradiated under a longitudinally polarized EM field. The longitudinally polarized field results in intrasubband transitions [13, 14], whereas a transversely polarized field results in intersubband transitions [10–12]. Both types of transition come from absorbing/emitting photons of quantum confined electrons. However, when an external longitudinally polarized field irradiates a finite range of a quantum wire, the displacement symmetry along the wire is violated so that the longitudinal momentum is not a conservative quantity and reflection must arise in general. The transport for a quantum wire under a longitudinally polarized EM field has been studied by a nonequilibrium Green function approach [13], where the interaction of the confined electron with a longitudinal photon has been described in a dipole approximation. However, the authors have only considered the particular case of a two-sublevel wire and the final results for the conductance or current must be time-averaged. This system has been also studied [14] by using a vector potential to represent the EM field, but calculation in this method allows only single incident electron mode. Furthermore, a common simplification in this system is to assume that a uniform oscillation field exists for x-independent space [7]. In this paper we will use the Floquet scattering approach to solve the single-particle time-dependent Schrödinger equation, in which the interaction term is described in a dipole approximation. After matching the wavefunctions at the interfaces between regions with and without field irradiation, we derive straightforwardly some infinite matrix equations which describe the multi-photon sideband transitions for the system. Then we numerically calculate the conductance as a function of electron incident energy with different field amplitude, frequency and irradiating length, respectively.

The Floquet scattering theory has had some success in treating a laser-driven quantum well system with dipole-type potentials [15, 16]. The quantum well situation is similar to a quantum wire under a longitudinally polarized EM field irradiation except for the difference in the boundary (interface) condition between the two cases. So we extend the Floquet scattering method to our quantum wire time-dependent problem; to our knowledge this extension has seldom been done previously [14].

The paper is arranged as follows. In section 2 the time-dependent Schrödinger equation for the system is derived and its Floquet scattering solutions in the different regions of the quantum wire are presented. Then the multi-photon sideband scattering equations relating to the scattering matrix are obtained by matching the solutions at the two interfaces. In section 3

we present respectively some numerical examples of the conductance as a function of incident electron energy for different field amplitude, frequency and length, and discuss the numerical results. And finally, section 4 presents a summary of the paper.

2. Model and method

The model system under investigation is an ideal long quantum wire (electron waveguide) adiabatically connecting two reservoirs at each end. The x-axis is longitudinally along the wire, and the y-axis is in the transverse direction. A longitudinally polarized external EM field with wavevector along the z-axis irradiates a finite range ($0 \leqslant x \leqslant L$) of the wire in an unspecified way. The electric component of the field is described by

$$\vec{E}(t) = \varepsilon \cos(\omega t)\theta(L/2 - |x|)\hat{x}, \tag{1}$$

where ε and ω are the amplitude and angular frequency of the field, respectively, $\hat{x}$ is the unit vector in the x direction (polarized direction), and $\theta(\cdot)$ is the step function.

2.1. Time-dependent Schrödinger equation

When the range of the irradiating field L is assumed to be comparable with the phase-breaking length of electrons, the entire transmission process is coherent and can be described by a time-dependent Schrödinger equation. The two reservoirs at both ends of the quantum wire can be taken to be free from the time-modulation effects so that the distribution of the incident electrons is well determined. Therefore, at low temperature and in the ballistic regime we adopt the effective-mass free-electron model which neglects the charging effect and imperfections. Hence in the dipole approximation [16] the single-particle time-dependent Schrödinger equation reads

$$\mathrm{i}\hbar\frac{\partial}{\partial t}\Psi(x, y, t) = \left[-\frac{\hbar^2}{2m^*}\left(\frac{\partial^2}{\partial x^2} + \frac{\partial^2}{\partial y^2}\right) + e\varepsilon x\cos(\omega t)\theta(L/2 - |x|) + v(y)\right]\Psi(x, y, t), \tag{2}$$

where m^* and e are the effective mass and the charge of an electron, respectively, and $v(y)$ is in the form of either a hard-wall potential or a parabolic one which confines electrons to the wire and to the reservoirs. In this paper, we use a parabolic potential $v(y) = \omega_0^2 y^2$ to define the quantum wire, where ω_0 is the strength of confinement.

The dipole-type finite-range time-dependent potential in equation (2) is uniform in the transverse direction and does not induce intersubband transitions, leaving the subband index unchanged. Thus, for the nth subband electron incident along the x-direction the scattering wavefunction can be written as

$$\Psi(x, y, t) = \psi(x, t)\phi_n(y), \tag{3}$$

where $\phi_n(y)$ is the transverse wavefunction corresponding to the nth subband with energy levels $\epsilon_n = (2n+1)\hbar\omega_0$. Inserting equation (3) into (2), we obtain a time-dependent one-dimensional Schrödinger equation

$$\mathrm{i}\hbar\frac{\partial}{\partial t}\psi(x, t) = \left[-\frac{\hbar^2}{2m^*}\frac{\partial^2}{\partial x^2} + V(x, t)\right]\psi(x, t), \tag{4}$$

where $V(x, t) = [\epsilon_n + e\varepsilon x\cos(\omega t)]\theta(L/2 - |x|)$ is the effective longitudinal scattering potential which is time dependent with the period of $T = 2\pi/\omega$. This type of equation has been used in describing many aspects [17] of interaction of matter with an EM field and has been treated by time-dependent perturbation theory [18–20] for driving a quantum well system.

2.2. Floquet scattering solution

The non-perturbative general solution of equation (4) in the range of $|x| < L/2$ may be written [15, 16] as a superposition of Floquet states

$$\psi(x,t) = \mathrm{e}^{-\mathrm{i}(E+\frac{e^2\varepsilon^2}{4m^*\omega^2})t/\hbar} \sum_{l=-\infty}^{\infty} \left[a_l \mathrm{e}^{\mathrm{i}k_l(x-e\varepsilon\cos\omega t/m^*\omega^2)} + b_l \mathrm{e}^{-\mathrm{i}k_l(x-e\varepsilon\cos\omega t/m^*\omega^2)}\right] \times \exp\left[-\mathrm{i}\left(l\omega t + \frac{e\varepsilon x\sin\omega t}{\hbar\omega} - \frac{e^2\varepsilon^2\sin 2\omega t}{8\hbar m^*\omega^3}\right)\right], \tag{5}$$

where a_l and b_l are the two scattering coefficients to be determined, and $\psi(x,t)$ is of the form $\exp(-\mathrm{i}E_\mathrm{F}t/\hbar)u(t)$ with $u(t) = u(t+2\pi/\omega)$ which is the characteristic for a Floquet state. A Floquet state is the analogue to a Bloch state when replacing a spatially periodic potential with a time periodic one. The quasimomentum of the Bloch state becomes the quasienergy E_F of the Floquet state. From equation (5) we find the Floquet eigenenergy $E_\mathrm{F} = E + e^2\varepsilon^2/4m^*\omega^2$, where E is the total energy constant. The sideband wavevectors k_l in solution (5) satisfy the relation

$$\hbar^2 k_l^2/2m^* = E - \epsilon_n + l\hbar\omega. \tag{6}$$

Using the identities $\exp(-\mathrm{i}x\sin\omega t) = \sum_m J_m(x)\exp(-\mathrm{i}m\omega t)$, $\exp(-\mathrm{i}x\cos\omega t) = \sum_m(-\mathrm{i})^m J_m(x)\exp(-\mathrm{i}m\omega t)$, and $J_m(-x) = (-1)^m J_m(x)$, where $J_m(x)$ is the Bessel function of the first kind, solution (5) can be rewritten as

$$\psi(x,t) = \sum_{m=-\infty}^{\infty}\sum_{l=-\infty}^{\infty}\sum_{\alpha,\beta=-\infty}^{\infty}(-\mathrm{i})^\alpha\left[a_l\mathrm{e}^{\mathrm{i}k_l x} + (-1)^\alpha b_l \mathrm{e}^{-\mathrm{i}k_l x}\right] \times I_l(\alpha,\beta)J_{m-l-\alpha+2\beta}\left(\frac{e\varepsilon x}{\hbar\omega}\right)\mathrm{e}^{-\mathrm{i}E_m t/\hbar}, \tag{7}$$

where we have used the abbreviation

$$I_l(\alpha,\beta) = J_\alpha\left(\frac{e\varepsilon k_l}{m^*\omega^2}\right)J_\beta\left(\frac{e^2\varepsilon^2}{8\hbar m^*\omega^3}\right), \tag{8}$$

and $E_m = E_\mathrm{F} + m\hbar\omega$ are multi-photon sidebands with energy spacing of $\hbar\omega$.

Since electrons incident into the field irradiated region will be scattered inelastically into Floquet sidebands, the wavefunctions outside the scatter region must consist of multiple Floquet sidebands in order to match the continuous condition at interfaces of $x = \pm L/2$. The potential in both sides of the wire is zero, so we simply assume that the incoming and outgoing waves in both sides are superpositions of an infinite number of sidebands with energy spacing of $\hbar\omega$. Therefore, the wavefunctions in these two free particle regions are

$$\psi(x,t) = \sum_{m=-\infty}^{\infty}(A_m^\mathrm{i}\mathrm{e}^{\mathrm{i}q_m x} + A_m^\mathrm{o}\mathrm{e}^{-\mathrm{i}q_m x})\mathrm{e}^{-\mathrm{i}E_m t/\hbar}, \qquad x < -L/2 \tag{9}$$

and

$$\psi(x,t) = \sum_{m=-\infty}^{\infty}(B_m^\mathrm{i}\mathrm{e}^{-\mathrm{i}q_m x} + B_m^\mathrm{o}\mathrm{e}^{\mathrm{i}q_m x})\mathrm{e}^{-\mathrm{i}E_m t/\hbar}, \qquad x > L/2 \tag{10}$$

respectively. Here A_m^i and B_m^i are the probability amplitudes of the incoming waves from left or right, respectively, while A_m^o and B_m^o are those of the outgoing waves. The incoming waves are divided into different zones with index m: $E_m = E_0 + m\hbar\omega$, where $E_0 \in [\hbar\omega_0, 3\hbar\omega_0)$ is the Floquet energy of the propagating mode with lowest energy, $\hbar^2 q_m^2/2m^* = E_0 - \epsilon_n + m\hbar\omega$.

2.3. Scattering coefficients

The Floquet eigenenergy E_{F} in equation (7) can be determined up to an arbitrary integer multiplied by $\hbar\omega$; shifting E_{F} by $m\hbar\omega$ does not change the wavefunction $\psi(x,t)$ due to $E_m = E_{\mathrm{F}} + m\hbar\omega$. For convenience, we choose E_{F} within the lowest zone, $E_{\mathrm{F}} = E_0$.

The wavefunctions (7)–(10) and their first derivatives must be continuous at the interfaces of $x = -L/2$ and $X = L/2$, respectively. These conditions lead to the following infinite equations after some algebraic operations:

$$\sum_{l=-\infty}^{\infty}\sum_{\alpha,\beta=-\infty}^{\infty}(\mathrm{i})^{\alpha}\left\{(-1)^{(m-l)}\left[\mathrm{i}(q_m+k_l)J_{m-l-\alpha+2\beta}\left(\frac{e\varepsilon L}{2\hbar\omega}\right)+\left(\frac{e\varepsilon}{2\hbar\omega}\right)\left(J_{m-l-\alpha+2\beta+1}\left(\frac{e\varepsilon L}{2\hbar\omega}\right)\right.\right.\right.$$
$$\left.\left.-J_{m-l-\alpha+2\beta-1}\left(\frac{e\varepsilon L}{2\hbar\omega}\right)\right)\right]\mathrm{e}^{-\mathrm{i}k_l L/2}\pm(-1)^{\alpha}\left[\mathrm{i}(q_m-k_l)J_{m-l-\alpha+2\beta}\left(\frac{e\varepsilon L}{2\hbar\omega}\right)\right.$$
$$\left.+\left(\frac{e\varepsilon}{2\hbar\omega}\right)\left(J_{m-l-\alpha+2\beta+1}\left(\frac{e\varepsilon L}{2\hbar\omega}\right)-J_{m-l-\alpha+2\beta-1}\left(\frac{e\varepsilon L}{2\hbar\omega}\right)\right)\right]\mathrm{e}^{\mathrm{i}k_l L/2}\Bigg\}I_l(\alpha,\beta)$$
$$\times\left[a_l\pm(-1)^{(m-l)}b_l\right]=2\mathrm{i}q_m\mathrm{e}^{-\mathrm{i}q_m L/2}(A_m^{\mathrm{i}}\pm B_m^{\mathrm{i}}). \tag{11}$$

If the incoming amplitudes A_m^{i} and B_m^{i} are given, then we can use equation (11) to determine the coefficients a_l and b_l. Therefore, the amplitudes of the outgoing waves are given by

$$A_m^{\mathrm{o}}=\sum_{l=-\infty}^{\infty}\sum_{\alpha,\beta=-\infty}^{\infty}(-\mathrm{i})^{\alpha}\left[a_l\mathrm{e}^{-\mathrm{i}k_l L/2}+(-1)^{\alpha}b_l\mathrm{e}^{\mathrm{i}k_l L/2}\right]J_{m-l-\alpha+2\beta}\left(\frac{-e\varepsilon L}{2\hbar\omega}\right)$$
$$\times I_l(\alpha,\beta)\mathrm{e}^{-\mathrm{i}q_m L/2}-A_m^{\mathrm{i}}\mathrm{e}^{-\mathrm{i}q_m L}, \tag{12}$$

and

$$B_m^{\mathrm{o}}=\sum_{l=-\infty}^{\infty}\sum_{\alpha,\beta=-\infty}^{\infty}(-\mathrm{i})^{\alpha}\left[a_l\mathrm{e}^{\mathrm{i}k_l L/2}+(-1)^{\alpha}b_l\mathrm{e}^{-\mathrm{i}k_l L/2}\right]J_{m-l-\alpha+2\beta}\left(\frac{e\varepsilon L}{2\hbar\omega}\right)$$
$$\times I_l(\alpha,\beta)\mathrm{e}^{-\mathrm{i}q_m L/2}-B_m^{\mathrm{i}}\mathrm{e}^{-\mathrm{i}q_m L}. \tag{13}$$

After these quantities of interest are obtained, a Landauer–Büttiker-type [19] scattering matrix can be constructed to study the quantum transport property of the system. In practice we can use a truncated version of equation (11) to obtain its numerical solution with required accuracy.

2.4. Scattering matrix

The outgoing wave amplitude equations (12) and (13) can be expressed in matrix form:

$$\begin{pmatrix}A^{\mathrm{o}}\\B^{\mathrm{o}}\end{pmatrix}=S\begin{pmatrix}A^{\mathrm{i}}\\B^{\mathrm{i}}\end{pmatrix}, \tag{14}$$

where A^{i}, B^{i} and A^{o}, B^{o} are the incoming and outgoing (including the associated evanescent Floquet sidebands) amplitude vectors, respectively. The scattering matrix S consists of all the probability amplitudes which connect the incoming wave amplitude vectors A^{i} and B^{i} to outgoing wave amplitude ones A^{o} and B^{o} (see the appendix).

If we keep only the propagating modes, then we obtain the scattering matrix $\bar{S}$ which satisfies

$$\begin{pmatrix}\bar{A}^{\mathrm{o}}\\\bar{B}^{\mathrm{o}}\end{pmatrix}=\bar{S}\begin{pmatrix}\bar{A}^{\mathrm{i}}\\\bar{B}^{\mathrm{i}}\end{pmatrix}, \tag{15}$$

and can be determined by the transmission and reflection amplitudes for the propagating modes

$$\bar{S} = \begin{pmatrix} \bar{R} & \bar{T}' \\ \bar{T}^{\circ} & \bar{R}' \end{pmatrix} = \begin{pmatrix} r_{00} & r_{01} & \cdots & t'_{00} & t'_{01} & \cdots \\ r_{10} & r_{11} & \cdots & t'_{10} & t'_{11} & \cdots \\ \cdot & \cdot & & \cdot & \cdot & \\ t_{00} & t_{01} & \cdots & r'_{00} & r'_{01} & \cdots \\ t_{10} & t_{11} & \cdots & r'_{10} & r'_{11} & \cdots \\ \cdot & \cdot & & \cdot & \cdot & \end{pmatrix}, \tag{16}$$

where r_{mn} and t_{mn} are the reflection and transmission amplitudes, respectively, for modes incident from the left; r'_{mn} and t'_{mn} are similar quantities for modes incident from the right. Here $m, n \in [0, \infty]$ since matrix $\bar{S}$ contains only the reflection and transmission amplitudes of the propagating modes. Elements such as $t_{-1,0}$, $r_{-1,0}$ in matrix S correspond to probability amplitudes describing an electron with incident energy E_0 being scattered into the evanescent mode E_{-1}.

From the scattering matrix one can obtain the total transmission coefficient

$$T = \sum_{n=0}^{\infty} \sum_{m=0}^{\infty} \frac{q_m}{k_n} |t_{mn}|^2. \tag{17}$$

If we consider a single electron wave incident from one direction (say the left) with a fixed Fermi energy E_0 and wavevector q_0, there is only one element, A_0^{i}, that is nonzero in the incoming amplitude vector, and the transmission coefficient T calculated from equation (23) involves only t_{n0} ($m = 0$ and n varies over all the transmitted propagating sidebands) [14]. If the incident energy belongs to a higher energy zone m [$(2m+1)\hbar\omega_y \leqslant E_{\mathrm{in}} < (2(m+1)+1)\hbar\omega_y$], we use t_{ml} in the corresponding column in the S matrix. According to the Landauer–Büttiker formula [19], the total conductance of the quantum wire is

$$G = \frac{2e^2}{h} T. \tag{18}$$

The conductance G can be measured in experiments [1, 2, 9].

2.5. Transmission calculation

The algebraic equation (11) for the coefficients a_l and b_l can be divided into two components for odd and even order m, respectively. However, the odd m component contribution is at least one order less than that of the even m one through our analysis, and can be neglected. To simplify the calculation work without loss of the basic physics of the transmission behaviour, here we reduce the even m component of equation (11) as

$$\begin{aligned} \sum_{l=-\infty}^{\infty} \sum_{\alpha,\beta=-\infty}^{\infty} \Bigg\{ (\mathrm{i})^{\alpha} (-1)^{l} \Bigg[\mathrm{i}(q_m + k_l) J_{m-l-\alpha+2\beta}\left(\frac{e\varepsilon L}{2\hbar\omega}\right) + \left(\frac{e\varepsilon}{2\hbar\omega}\right) \Bigg(J_{m-l-\alpha+2\beta+1}\left(\frac{e\varepsilon L}{2\hbar\omega}\right) \\ - J_{m-l-\alpha+2\beta-1}\left(\frac{e\varepsilon L}{2\hbar\omega}\right) \Bigg) \Bigg] \mathrm{e}^{-\mathrm{i}k_l L/2} \pm (-\mathrm{i})^{\alpha} \Bigg[\mathrm{i}(q_m - k_l) J_{m-l-\alpha+2\beta}\left(\frac{e\varepsilon L}{2\hbar\omega}\right) \\ + \left(\frac{e\varepsilon}{2\hbar\omega}\right) \Bigg(J_{m-l-\alpha+2\beta+1}\left(\frac{e\varepsilon L}{2\hbar\omega}\right) - J_{m-l-\alpha+2\beta-1}\left(\frac{e\varepsilon L}{2\hbar\omega}\right) \Bigg) \Bigg] \mathrm{e}^{\mathrm{i}k_l L/2} \Bigg\} I_l(\alpha, \beta) \\ \times \left[a_l \pm (-1)^{l} b_l \right] = 2\mathrm{i} q_m \mathrm{e}^{-\mathrm{i}q_m L/2} (A_m^{\mathrm{i}} \pm B_m^{\mathrm{i}}). \end{aligned} \tag{19}$$

To solve equation (19), let us first introduce some relevant matrices whose elements are defined in the following way:

$$(Q_s^{\pm})_{ml} = \sum_{\alpha,\beta=-\infty}^{\infty} \left\{ (\mathrm{i})^{\alpha}(-1)^{l} \left[\mathrm{i}(q_m + k_l) J_{m-l-\alpha+2\beta}\left(\frac{e\varepsilon L}{2\hbar\omega}\right) + \left(\frac{e\varepsilon}{2\hbar\omega}\right)\left(J_{m-l-\alpha+2\beta+1}\left(\frac{e\varepsilon L}{2\hbar\omega}\right) - J_{m-l-\alpha+2\beta-1}\left(\frac{e\varepsilon L}{2\hbar\omega}\right)\right)\right] \mathrm{e}^{-\mathrm{i}k_l L/2} \pm (-\mathrm{i})^{\alpha} \left[\mathrm{i}(q_m - k_l) J_{m-l-\alpha+2\beta}\left(\frac{e\varepsilon L}{2\hbar\omega}\right) + \left(\frac{e\varepsilon}{2\hbar\omega}\right)\left(J_{m-l-\alpha+2\beta+1}\left(\frac{e\varepsilon L}{2\hbar\omega}\right) - J_{m-l-\alpha+2\beta-1}\left(\frac{e\varepsilon L}{2\hbar\omega}\right)\right)\right] \mathrm{e}^{\mathrm{i}k_l L/2} \right\} I_l(\alpha, \beta), \tag{20}$$

$$(Q_r)_{ml} = 2\mathrm{i}q_m \mathrm{e}^{-\mathrm{i}q_m L/2}\delta_{m,l}, \tag{21}$$

$$(Q_1^{\pm})_{ml} = \sum_{\alpha,\beta=-\infty}^{\infty} \mathrm{e}^{-\mathrm{i}(q_m+k_l)L/2}(\mp\mathrm{i})^{\alpha}(\pm 1)^{l} J_{m-l-\alpha+2\beta}\left(\frac{-e\varepsilon L}{2\hbar\omega}\right) I_l(\alpha, \beta), \tag{22}$$

$$(Q_2^{\pm})_{ml} = \sum_{\alpha,\beta=-\infty}^{\infty} \mathrm{e}^{-\mathrm{i}(q_m-k_l)L/2}(\mp\mathrm{i})^{\alpha}(\pm 1)^{l} J_{m-l-\alpha+2\beta}\left(\frac{-e\varepsilon L}{2\hbar\omega}\right) I_l(\alpha, \beta), \tag{23}$$

$$(Q_i)_{ml} = \mathrm{e}^{-\mathrm{i}q_m L}\delta_{m,l}, \tag{24}$$

$$C_l^{\pm} = \left[a_l \pm (-1)^{(-l)} b_l\right]. \tag{25}$$

Using the above definitions, we obtain the following matrix equation for the Floquet scattering matrix S (see the appendix):

$$\begin{pmatrix} \mathbf{A}^{\mathrm{o}} \\ \mathbf{B}^{\mathrm{o}} \end{pmatrix} = \begin{pmatrix} \mathbf{Q}_{AA} & \mathbf{Q}_{AB} \\ \mathbf{Q}_{BA} & \mathbf{Q}_{BB} \end{pmatrix} \begin{pmatrix} \mathbf{A}^{\mathrm{i}} \\ \mathbf{B}^{\mathrm{i}} \end{pmatrix} = S \begin{pmatrix} \mathbf{A}^{\mathrm{i}} \\ \mathbf{B}^{\mathrm{i}} \end{pmatrix}. \tag{26}$$

Each element S_{mn} of matrix S gives the probability amplitude that the electron is scattered from Floquet sideband n to sideband m [$m, n \in (-\infty, \infty)$]. If we keep only the propagating modes [$m, n \in [0, \infty)$], we then extract it from S matrix to obtain $\bar{S}$ as equation (21).

The finiteness in the range of the applied EM field breaks the translational invariance, and hence allows the coherent inelastic scattering not to conserve the longitudinal momentum. On the other hand, the uniformity of the field in the transverse direction does not induce intersubband transitions and so each occupied subband contributes independently to the total transmission amplitudes. Thus it suffices for our purposes here to present the transmission amplitude of only one subband, which we take to be the lowest one.

3. Numerical results and discussion

In our numerical examples, the quantum wire is taken to be that in a high mobility GaAs–$Al_xGa_{1-x}As$ heterostructure [1, 2] with a typical electron density $n \sim 2.5 \times 10^{11}$ cm^{-2} and $m^* = 0.067m_0$, where m_0 is the free electron mass. Correspondingly, we choose an energy unit $E^* = \hbar^2 k_{\mathrm{F}}^2/(2m^*) = 9$ meV, a length unit $a^* = 1/k_{\mathrm{F}} = 79.6$ Å, a frequency unit $\omega^* = E^*/\hbar = 13.6$ THz, and the field amplitude ε in units of 11.3 kV cm^{-1}. In the following, the dependence of the electron transmission probability T on the incident electron energy E is more conveniently plotted as the dependence of T on X, where the integral value of $X = E/\Delta\epsilon$ gives the number of propagating channels ($\Delta\epsilon = 2\hbar\omega_0$ is the subband energy-level spacing).

First, we present the numerically calculated T dependence on X in figures 1(a)–(c) for three different field amplitudes of $\varepsilon = 0.0025$ ($\simeq$28.3 V cm^{-1}), 0.005 ($\simeq$56.5 V cm^{-1}), 0.015 ($\simeq$169.7 V cm^{-1}), respectively. Here we have fixed the field frequency $\omega = 0.042$ ($\simeq$0.574 THz, which is typical for current experiments [21]) and the length of the field irradiation $L = 60$ ($\simeq$0.5 μm), and chosen the strength of the lateral confinement $\hbar\omega_0 = 0.035$ for the quantum wire such that the subband energy-level spacing $\Delta\epsilon = 0.07$. Besides the

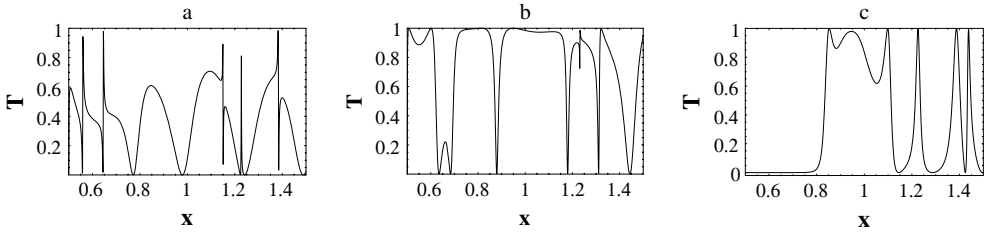

Figure 1. Transmission probability T as a function of X for different field amplitudes of (a) $\varepsilon = 0.0025$ ($\simeq$28.3 V cm^{-1}), (b) $\varepsilon = 0.005$ ($\simeq$56.5 V cm^{-1}), and (c) $\varepsilon = 0.015$ ($\simeq$169.7 V cm^{-1}). The field frequency and irradiation length are chosen to be $\omega = 0.042$ and $L = 60$ ($\simeq$0.5 μm), respectively, and the confinement strength is $\omega_y = 0.035$.

incident channel $E = E_0$, Floquet sidebands both above and below E_0 are taken into account: $E_m = E_0 + m\hbar\omega$ with $m = 0, \pm 2, \pm 4$.

From figure 1 we can see the variation of transmission T between 0 and 1, in which the variation pattern depends on the field amplitude. With the relatively small field amplitude $\varepsilon = 0.0025$ shown in figure 1(a), the transmission pattern shows several transmission dip structures. According to equation (6) we find that the sideband wavevector k_l ($l \geqslant 1$) always corresponds to a propagating mode within our numerical interval, but k_0 begins to be a propagating state and requires $X \sim 0.525$. In this case the quantum wire ensures that there exists a quasi-bound state, which results in an asymmetric Fano resonance where a sharp dip is followed by a peak. As X increases, the sideband wavevector k_{-1} is a propagating state when $X > 0.64$. Therefore, there is also a Fano dip associating with another quasi-bound state. We can also identify two other Fano resonances where a peak is followed by a sharp dip at $X = 1.15$ and 1.38, respectively, which may result from higher sidebands. In addition to the asymmetric Fano dips for the transmission, there exist symmetric dip structures at $X \simeq 0.76, 0.98$, and 1.25, respectively, in figure 1(a). This phenomenon can be interpreted as a Rabi oscillation interference effect between different sidebands. Furthermore, with an intermediate value of the field amplitude $\varepsilon = 0.005$ shown in figure 1(b), there are only a few symmetric dips at $X \simeq 0.65, 0.68, 0.88, 1.17, 1.32$ and 1.45, respectively. The only asymmetric nonzero dip followed by a peak at $X = 1.23$ may be identified as a Fano resonance. However, as the amplitude of field increases to a relative large value of $\varepsilon = 0.015$, as shown in figure 1(c) the transmission remains at zero until $X \sim 0.81$. The phenomenon can be interpreted as follows. The sideband wavevector k_1 corresponds to an evanescent state when $X < 0.81$, so there is no propagating mode in the field-irradiated region and the transmission equals zero. As $X > 0.81$, a new channel begin to open and it enhances the reflection of electrons out of the field-irradiated region, and the transmission begins to oscillate.

From the numerical examples of figure 1 we conclude that under certain frequency field irradiation the transmission dependence on the incident energy of a quantum wire is sensitive to the field amplitude. The transmission shows mainly asymmetric Fano resonance structure for a relatively small amplitude, while for a relatively larger amplitude it displays a pure symmetric Rabi oscillation pattern. It seems that for the intermediate value of the field amplitude of $\varepsilon = 0.015$ the transmission shows a transition state from Fano resonance to Rabi oscillation but with a maximum average probability. In the remaining part of this section we will use an intermediate value of the field amplitude case (figure 1(b)) as a comparative reference.

Next, we present the numerically calculated T dependence on X in figures 2(a)–(c) for three different field frequencies of $\omega = 0.028$ ($\simeq$0.383 THz), 0.042 ($\simeq$0.574 THz) and 0.421 ($\simeq$5.75 THz), respectively. Here we have chosen $\varepsilon = 0.005$, and the field irradiation length

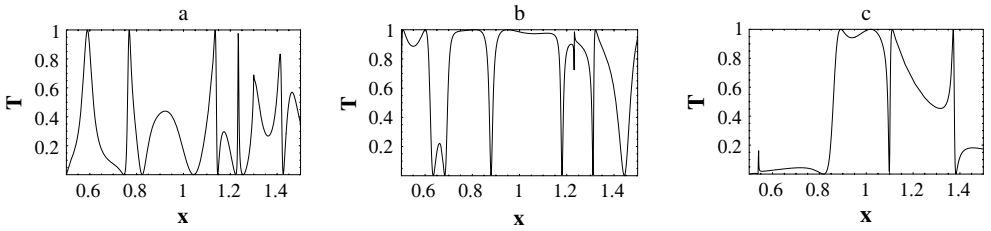

Figure 2. Transmission probability T as a function of X for different field frequencies (a) $\omega = 0.035$ ($\simeq$0.478 THz), (b) $\omega = 0.042$ ($\simeq$0.574 THz), and (c) $\omega = 0.049$ ($\simeq$0.669 THz). The field amplitude is chosen to be $\varepsilon = 0.005$, and the irradiation length and the confinement strength are the same as those in figure 1.

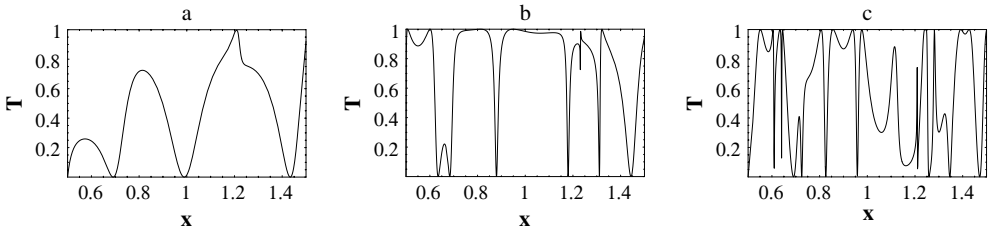

Figure 3. Transmission probability T as a function of X for different field irradiation lengths of (a) $L = 30$ ($\simeq$0.25 μm); (b) $L = 60$ ($\simeq$0.5 μm), and (c) $L = 120$ ($\simeq$1 μm). The field frequency is $\omega = 0.042$, and the field amplitude and the confinement strength are the same as those in figure 2.

and the confinement strength are the same as those in figure 1. With a relatively small field frequency as shown in figure 2(a), the transmission pattern is more symmetric than that in figure 2(b) with an intermediate value of the field frequency. However, as shown in figure 2(c), the transmission remains almost zero until $X \sim 0.81$, as that in figure 1(c), with the same physical reason. But it shows clearly a Fano resonance at $X \simeq 1.38$ where a sharp peak is followed by a dip. This is also from a transition between a propagating state and a quasi-bound state.

Finally, we investigate the influence of the field irradiation length on the transmission. We present the calculated T as a function of X in figures 3(a)–(c) for different field irradiation lengths of $L = 30$ ($\simeq$0.25 μm), 60 ($\simeq$0.5 μm) and 120 ($\simeq$1 μm), respectively. Here we have chosen the field frequency $\omega = 0.042$, and the field amplitude is the same as that in figure 2. We note that for a relatively short irradiation length of $L = 30$ the transmission exhibits slow oscillation with a few wide dips as shown in figure 3(a). This may result mainly from the pure Rabi oscillations due to the short L. Interestingly, as shown in figures 3(b) and (c), with a longer L the transmission pattern oscillate more rapidly while the dip structures become more pronounced and the widths of the dips are narrower. So in the case of long L both Fano and Rabi resonance may be effective.

Lastly, we discuss the possibility of the experimental observation of the above effects based on our model system. The experimental setup based on a 2DEG for this kind of measurement has been proposed in [14], which my be suitable for our purpose. However, two requirements need to be fulfilled for observation. First, the bolometric effect due to absorption of photons in the quantum wire has to be suppressed or totally eliminated, because the transport characteristics may be affected by the bolometric effect when the wire is exposed to the incident EM field. Second, in order to increase the coupling between the electrons and

the photons by breaking the longitudinal translational invariance, the length of the region L acted on by the EM field needs to be shorter than the wavelength of the incident field. Thus the coupling between the conduction electrons and the photon field can be much enhanced for the observation.

4. Summary and conclusion

In summary, we have presented a generic Floquet scattering approach that allows us to obtain the Floquet eigenenergy and the scattering matrix for a quantum wire under a longitudinally polarized EM field irradiation within a finite range. The electron transmission dip structures result from the interaction of electrons with the electromagnetic field. Quasi-bound states can serve as an electron reservoir when an electromagnetic field is applied and electrons can drop there from the propagating modes by photon emission, in which form a Fano resonance. Rabi oscillations and interference effects of sidebands result in the abundance structure of the transmission. But the structure of the transmission is sensitive to the field amplitude and frequency as well as the irradiation length. Fano resonance may be used to 'probe' the semiconductor energy spectrum, and measure mesoscopic system parameters such as width and band structure. In addition, this sharp peak–dip resonance pattern (sometimes only a dip appears) also allows sensitive control of the transport property and may be useful for designing fast response switching quantum heterostructures. On the other hand, one may also sensitively control the transport of a heterostructure through the external electromagnetic field parameters.

Acknowledgments

This work was supported by the Nature Science Foundation of China (NSFC) under Grant No. 10574042 and by the Research Foundation of Hunan Education Commission under Grant No. 04A031.

Appendix. Derivation of the Floquet S matrix

In this appendix we show how to construct the Floquet S matrix using matrix format. According to the definitions of equations (20)–(25), equation (19) can then be expressed in matrix form:

$$\mathbf{Q}_s^{\pm} \cdot \mathbf{C}^{\pm} = \mathbf{Q}_r \cdot (\mathbf{A}^{\mathrm{i}} \pm \mathbf{B}^{\mathrm{i}}). \tag{A.1}$$

When the state matrix $\mathbf{Q}_s^{\pm}$ is not singular, we can take the inverse and the coefficient vector $\mathbf{C}^{\pm}$ becomes

$$\mathbf{C}^{\pm} = (\mathbf{Q}_s^{\pm})^{-1} \cdot \mathbf{Q}_r \cdot (\mathbf{A}^{\mathrm{i}} \pm \mathbf{B}^{\mathrm{i}}), \tag{A.2}$$

where the coefficients a_l and b_l are given by $a_l = (C_l^+ + C_l^-)/2$ and $b_l' = (-1)^l b_l = (C_l^+ - C_l^-)/2$. The coefficient vectors are given by

$$\begin{aligned}\mathbf{a} = \tfrac{1}{2}(\mathbf{C}^+ + \mathbf{C}^-) &= \tfrac{1}{2}\left[(\mathbf{Q}_s^+)^{-1} \cdot \mathbf{Q}_r \cdot (\mathbf{A}^{\mathrm{i}} + \mathbf{B}^{\mathrm{i}}) + (\mathbf{Q}_s^-)^{-1} \cdot \mathbf{Q}_r \cdot (\mathbf{A}^{\mathrm{i}} - \mathbf{B}^{\mathrm{i}})\right] \\ &= \tfrac{1}{2}\left[(\mathbf{Q}_s^+)^{-1} + (\mathbf{Q}_s^-)^{-1}\right] \cdot \mathbf{Q}_r \cdot \mathbf{A}^{\mathrm{i}} + \tfrac{1}{2}\left[(\mathbf{Q}_s^+)^{-1} - (\mathbf{Q}_s^-)^{-1}\right] \cdot \mathbf{Q}_r \cdot \mathbf{B}^{\mathrm{i}},\end{aligned} \tag{A.3}$$

and

$$\begin{aligned}\mathbf{b}' = \tfrac{1}{2}(\mathbf{C}^+ - \mathbf{C}^-) &= \tfrac{1}{2}\left[(\mathbf{Q}_s^+)^{-1} \cdot \mathbf{Q}_r \cdot (\mathbf{A}^{\mathrm{i}} + \mathbf{B}^{\mathrm{i}}) - (\mathbf{Q}_s^-)^{-1} \cdot \mathbf{Q}_r \cdot (\mathbf{A}^{\mathrm{i}} - \mathbf{B}^{\mathrm{i}})\right] \\ &= \tfrac{1}{2}\left[(\mathbf{Q}_s^+)^{-1} - (\mathbf{Q}_s^-)^{-1}\right] \cdot \mathbf{Q}_r \cdot \mathbf{A}^{\mathrm{i}} + \tfrac{1}{2}\left[(\mathbf{Q}_s^+)^{-1} + (\mathbf{Q}_s^-)^{-1}\right] \cdot \mathbf{Q}_r \cdot \mathbf{B}^{\mathrm{i}}.\end{aligned} \tag{A.4}$$

Now rewrite equations (12) and (13) for the outgoing wave amplitude vectors in matrix form:

$$\begin{aligned}\mathbf{A}^{\mathrm{o}} &= \mathbf{Q}_{c1}^{+}\cdot\mathbf{a}+\mathbf{Q}_{c2}^{-}\cdot\mathbf{b}'-\mathbf{Q}_{i}\cdot\mathbf{A}^{\mathrm{i}}\\ &= \left(\tfrac{1}{2}\left\{\mathbf{Q}_{c1}^{+}\cdot\left[(\mathbf{Q}_{s}^{+})^{-1}+(\mathbf{Q}_{s}^{-})^{-1}\right]+\mathbf{Q}_{c2}^{-}\cdot\left[(\mathbf{Q}_{s}^{+})^{-1}-(\mathbf{Q}_{s}^{-})^{-1}\right]\right\}\cdot\mathbf{Q}_{r}-\mathbf{Q}_{i}\right)\cdot\mathbf{A}^{\mathrm{i}}\\ &\quad+\left(\tfrac{1}{2}\left\{\mathbf{Q}_{c1}^{+}\cdot\left[(\mathbf{Q}_{s}^{+})^{-1}-(\mathbf{Q}_{s}^{-})^{-1}\right]+\mathbf{Q}_{c2}^{-}\cdot\left[(\mathbf{Q}_{s}^{+})^{-1}+(\mathbf{Q}_{s}^{-})^{-1}\right]\right\}\cdot\mathbf{Q}_{r}\right)\cdot\mathbf{B}^{\mathrm{i}}\\ &\equiv \mathbf{Q}_{AA}\cdot\mathbf{A}^{\mathrm{i}}+\mathbf{Q}_{AB}\cdot\mathbf{B}^{\mathrm{i}},\end{aligned}\tag{A.5}$$

$$\begin{aligned}\mathbf{B}^{\mathrm{o}} &= \mathbf{Q}_{c2}^{+}\cdot\mathbf{a}+\mathbf{Q}_{c1}^{-}\cdot\mathbf{b}'-\mathbf{Q}_{i}\cdot\mathbf{B}^{\mathrm{i}}\\ &= \left(\tfrac{1}{2}\left\{\mathbf{Q}_{c2}^{+}\cdot\left[(\mathbf{Q}_{s}^{+})^{-1}+(\mathbf{Q}_{s}^{-})^{-1}\right]+\mathbf{Q}_{c1}^{-}\cdot\left[(\mathbf{Q}_{s}^{+})^{-1}-(\mathbf{Q}_{s}^{-})^{-1}\right]\right\}\cdot\mathbf{Q}_{r}\right)\cdot\mathbf{A}^{\mathrm{i}}\\ &\quad+\left(\tfrac{1}{2}\left\{\mathbf{Q}_{c2}^{+}\cdot\left[(\mathbf{Q}_{s}^{+})^{-1}-(\mathbf{Q}_{s}^{-})^{-1}\right]+\mathbf{Q}_{c1}^{-}\cdot\left[(\mathbf{Q}_{s}^{+})^{-1}+(\mathbf{Q}_{s}^{-})^{-1}\right]\right\}\cdot\mathbf{Q}_{r}-\mathbf{Q}_{i}\right)\cdot\mathbf{B}^{\mathrm{i}}\\ &\equiv \mathbf{Q}_{BA}\cdot\mathbf{A}^{\mathrm{i}}+\mathbf{Q}_{BB}\cdot\mathbf{B}^{\mathrm{i}}.\end{aligned}\tag{A.6}$$

Therefore, combining these two equations results in equation (26).

References

[1] van Wees B J, van Houten H, Beenakker C W J, Williamson J G, Kouwenhoven L P, van der Mare D and Foxon C T 1988 *Phys. Rev. Lett.* **60** 848
[2] Yacoby A, Stormer H L, Wingreen N S, Pfeiffer L N, Baldwin K W and West K W 1996 *Phys. Rev. Lett.* **77** 4612
[3] Szafer A and Stone A D 1989 *Phys. Rev. Lett.* **62** 300
Rubio G, Agrait N and Vieira S 1996 *Phys. Rev. Lett.* **76** 2302
[4] Wang X R, Wang Y and Sun Z Z 2002 *Phys. Rev.* B **65** 193402
[5] Ogata M and Fukuyama H 1994 *Phys. Rev. Lett.* **73** 468
Sushkov O P 2001 *Phys. Rev.* B **64** 155319
[6] Platero G and Aguado R 2004 *Phys. Rep.* **395** 1
[7] Tang C S and Chu C S 1996 *Phys. Rev.* B **53** 4838
Tang C S, Tan Y H and Chu C S 2003 *Phys. Rev.* B **67** 205324
[8] Brouwer P W 1998 *Phys. Rev.* B **58** R10135
Mucciolo E R, Chamon C and Marcus C M 2002 *Phys. Rev. Lett.* **89** 146802
[9] Hu Q 1993 *Appl. Phys. Lett.* **62** 837
Feng S C and Hu Q 1993 *Phys. Rev.* B **48** 5354
[10] Tageman O, Gorelik L Y, Shekter R I and Jonson M 1997 *J. Appl. Phys.* **81** 285
[11] Blom S and Gorelik L Y 2001 *Phys. Rev.* B **64** 45320
[12] Zhou G, Yang M, Xiao X and Li Y 2003 *Phys. Rev.* B **68** 155309
[13] Li S-S and Xia J-B 2002 *J. Appl. Phys.* **91** 3227
[14] Tang C S and Chu C S 1999 *Phys. Rev.* B **60** 1830
[15] Wanger M 1996 *Phys. Rev. Lett.* **76** 4010
[16] Li W and Reichl L E 2000 *Phys. Rev.* B **62** 8269
[17] Martinez D F 2005 *Preprint* cond-mat/0501023
[18] Aguado R, Inarrea J and Platero G 1994 *Phys. Rev.* B **50** 4581
Aguado R and Platero G 1998 *Phys. Rev. Lett.* **81** 4971
[19] Büttiker M 1986 *Phys. Rev. Lett.* **57** 1761
Landauer R 1989 *J. Phys.: Condens. Matter* **1** 8099
[20] Bagwell P F and Lake R K 1992 *Phys. Rev.* B **46** 15329
[21] Qin H, Simmel F, Blick R H, Kotthaus J P, Wegscheider W and Bichler M 2001 *Phys. Rev.* B **63** 35320